

Solution Structure of Human and Bovine β_2 -Glycoprotein I Revealed by Small-angle X-ray Scattering

Michal Hammel¹, Manfred Kriechbaum¹, Anna Gries²
Gerhard M. Kostner³, Peter Laggner¹ and Ruth Prassl^{1*}

¹Institute of Biophysics and X-ray Structure Research of the Austrian Academy of Sciences Schmiedlstr. 6, A-8042 Graz Austria

²Institute of Physiology University of Graz Harrachgasse 21, A-8010 Graz Austria

³Institute of Medical Biochemistry, University of Graz, Harrachgasse 21, A-8010 Graz, Austria

β_2 -Glycoprotein I (β_2 GPI) is a highly glycosylated phospholipid-binding plasma protein comprised of four complement control protein (CCP) domains and a distinct fifth domain. The structural organisation of human and bovine β_2 GPI in aqueous solution was studied by small-angle X-ray scattering (SAXS). Low-resolution models that match the SAXS experimental data best were independently constructed by three different *ab initio* 3D-reconstruction algorithms. Similar elongated S-shaped models with distinct side-arms, which were correlated to the position of the carbohydrate chains, were restored from all three algorithms. Due to an additional glycosylation site located on the CCP2 domain of bovine β_2 GPI a small change in the characteristic SAXS parameters was observed, which coincided with results obtained from SDS-PAGE. In comparison to the human analogue the corresponding restored low-resolution models displayed a similar S-shape with less bending in the middle part.

As the experimental SAXS curves fit poorly to the simulated scattering curves calculated from the crystallographic coordinates of human β_2 GPI, the crystal structure was modified. First, additional carbohydrate residues missing from the crystal structure were modelled. Second, on the basis of the low-resolution models, the J-shaped crystal structure was rotated between CCP3 and CCP2 assuming the greatest interdomain flexibility between these domains. An S-shaped model with a tilt angle of $\sim 60^\circ$ between CCP3 and CCP2 yielded the best fit to the experimental SAXS data. Since there is evidence that β_2 GPI can adopt different conformations, which reveal distinct differences in autoantibody recognition, our data clearly point to a reorientation of the flexible domains, which may be an essential feature for binding of autoantibodies.

© 2002 Elsevier Science Ltd. All rights reserved

Keywords: β_2 -glycoprotein I; apolipoprotein H; small angle X-ray scattering; low resolution modelling; complement control protein

*Corresponding author

Introduction

β_2 -Glycoprotein I (β_2 GPI), also designated as apolipoprotein-H, is a plasma glycoprotein either circulating free (0.2 mg/ml) or associated with lipoprotein fractions.^{1,2} *In vitro* studies have shown

Abbreviations used: aPLAs, autoimmune phospholipid autoantibodies; b- β_2 GPI, bovine β_2 -glycoprotein; CCP, complement control protein; h- β_2 GPI, human β_2 -glycoprotein; M_M , molecular mass; SAXS, small-angle X-ray scattering; β_2 GPI, β_2 -glycoprotein.

E-mail address of the corresponding author: ruth.prassl@oeaw.ac.at

that β_2 GPI plays a triggering role in the blood coagulation cascade,³ in platelet aggregation^{4,5} and in the course of thrombotic diseases.^{3,6} β_2 GPI is a highly glycosylated protein consisting of a single polypeptide chain (326 amino acid residues) with $\sim 19\%$ (w/w) carbohydrates attached to N-linked glycosylation sites.^{7,8} An elongated J-shaped arrangement of four complement control protein (CCP) modules and a distinct C-terminal domain V with overall protein dimensions of 13.2 nm \times 7.2 nm \times 2.0 nm was found by X-ray crystallography.^{9,10} The five domains are joined by short interdomain linkers. The linkers are bordered by two disulfide bonds and span only three (between

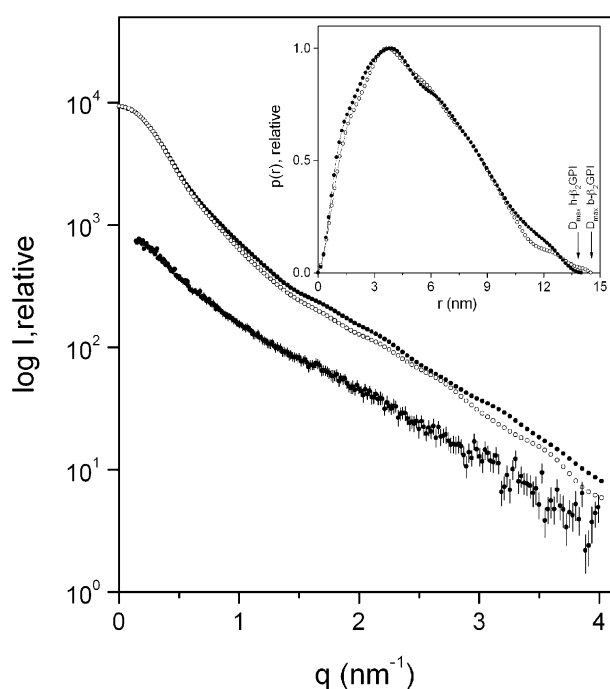


Figure 1. Experimental small-angle X-ray scattering raw data of h- β_2 GPI (dots with error bars) and the final desmeared scattering profiles for h- β_2 GPI (dots) and b- β_2 GPI (open circles) were processed as described in Materials and Methods. The inset shows the distance distribution functions $p(r)$ of h- β_2 GPI (dots) and b- β_2 GPI (open circles) evaluated by the program GNOM. The arrows indicate the estimated values of D_{\max} obtained from the $p(r)$ function.

CCP4 and domain V) or four residues (between the other domains). The four N-terminal CCP domains exhibit a conserved elliptically β -sandwich structure. They are highly homologous to each other and to the other representatives of this superfamily. In contrast, domain V folds into a central β -spiral with two small helices and carries a distinct positive charge in the proximity of the surface-exposed loop region.

β_2 GPI shows a high affinity for negatively charged ligands, including heparin, DNA,¹¹ cell membranes, endothelial cells,¹² macrophages¹³ or acidic phospholipids. Complexes formed by β_2 GPI and acidic phospholipids were suggested to act as antigens for autoimmune phospholipid autoantibodies (aPLAs) associated with clinical events such as antiphospholipid syndrome, lupus erythematosus, and recurrent fetal loss.^{14–16} The aberrant domain V is believed to bind to negatively charged phospholipids,^{17,18} whereas CCP1 and CCP4 are suggested to comprise aPLAs binding sites.^{19–21} Recent studies reveal that the N-terminal domains CCP1, CCP2, and CCP3 are involved in the formation of specific protein clusters,^{22,23} which can be recognized by aPLAs.²⁴ It has been argued that, upon epitope exposure in a ligand-associated state, the protein has a conformation different from that in the water-soluble state,^{21,25} in which β_2 GPI displays a reduced immunological

activity.²⁶ To address this issue, we carried out small-angle X-ray scattering (SAXS) experiments of β_2 GPI in aqueous solution, and we have restored three-dimensional structural models of β_2 GPI that were compared to the crystal structure solved recently by Bouma *et al.* and our group.^{9,10} The explicit differences of the overall shape between crystal and solution structure are attributed to carbohydrate units and to the flexibility of the CCP domains. The impact of a conceivable domain reorientation with respect to immunological activity and the structural differences between human β_2 GPI and its bovine analogue are discussed.

Results

Small-angle X-ray scattering parameters

SAXS raw data from human β_2 GPI (h- β_2 GPI) and the final desmeared SAXS profiles of h- β_2 GPI and bovine β_2 GPI (b- β_2 GPI) are shown in Figure 1. The radius of gyration (R_G) of β_2 GPI in aqueous solution decreases slightly with increasing concentration in the range $R_G = 4.3$ – 4.1 nm for h- β_2 GPI and $R_G = 4.4$ – 4.2 nm for b- β_2 GPI. This concentration-dependence of the radii of gyration is consistent with weak interparticle interactions. After extrapolation to infinite dilution, the final values of $R_G = 4.30$ nm for h- β_2 GPI and $R_G = 4.46$ nm for b- β_2 GPI from the Guinier approximation are obtained. These values are in good agreement with the R_G values derived from the $p(r)$ function of the scattering profiles of the extrapolated curves (see Table 1). The maximal particle dimensions derived from R_G and R_{xs} are $L = 13.6$ nm and 14.0 nm for h- β_2 GPI and b- β_2 GPI, respectively. The scattering profiles for h- β_2 GPI and b- β_2 GPI indicate similar shapes for both proteins (r.m.s = 0.04), which is seen also in the distance distribution functions $p(r)$ (Figure 1, inset).

The molecular masses (M_M), $M_M = 53.5$ kDa for h- β_2 GPI and $M_M = 58.0$ kDa for b- β_2 GPI estimated from $I(0)$ are in good agreement with values obtained from SDS-PAGE, i.e. 55.1 kDa and 58.1 kDa, respectively (Figure 2). The volumes for the hydrated protein $V = 96$ nm³ and $V = 110$ nm³ for h- β_2 GPI and b- β_2 GPI, respectively, are close to the volumes obtained from low-resolution models (see the next paragraph) and are twice the dry volume $V_d = 46$ nm³ calculated for the crystal structure of h- β_2 GPI (1C1Z.pdb) (Table 1). A large hydrated volume in comparison to the dry volume is characteristic for elongated proteins.²⁷ In our case, the hydrated volume is even enhanced by the high glycosylation rate of β_2 GPI. It can thus be concluded that the solution of β_2 GPI is monodisperse, and the scattering profiles can be further used for *ab initio* shape analyses.

Table 1. Experimental and model SAXS parameter

| Parameter | Human β_2 GPI | | | | | | Bovine β_2 GPI | | |
|--|---------------------|---------------------|-----------------------|-----------------------|---|--|----------------------|---------------------|-----------------------|
| | Exp. | DAMMIN ^a | DALAI_GA ^a | 1C1Z.pdb ^b | 1C1Z.pdb + carbo- hydrates (model 0°) ^b | 1C1Z.pdb + carbohydrates + rotation (model 130°) ^b | Exp. | DAMMIN ^a | DALAI_GA ^a |
| R_G (nm) | 4.30 ^c | 4.26 ± 0.01 | 4.21 ± 0.03 | 4.61 | 4.48 | 4.29 | 4.46 ^c | 4.34 ± 0.08 | 4.33 ± 0.06 |
| $R_G \rightarrow p(r)$ (nm) ^d | 4.32 ± 0.13 | | | 4.57 ± 0.03 | 4.25 ± 0.01 | 4.20 ± 0.03 | 4.37 ± 0.15 | | |
| R_{xs} (nm) ^e | 1.78 | | | 1.42 | 1.75 | 1.70 | 1.88 | | |
| L (nm) ^f | 13.6 | | | 15.2 | 14.3 | 13.6 | 14.0 | | |
| $D_{max} \rightarrow p(r)$ (nm) ^d | 13.9 | 13.4 ± 0.05 | 13.3 ± 0.2 | 14.9 | 14.9 | 13.9 | 14.5 | 13.7 ± 0.2 | 13.9 ± 0.5 |
| M_M (kDa) | 53.5 | | | 38.3 | 45.7 | 45.7 | 58.0 | | |
| V (nm ³) | 96 | 105 ± 2 | | 87 | 100 | 96 | 110 | 113 ± 2 | |
| r.m.s | | 0.0040 ± 0.0007 | 0.0017 ± 0.0002 | 0.13 | 0.015 | 0.004 | | 0.0019 ± 0.0018 | 0.0026 ± 0.0016 |

^a The values given are the average and standard error from ten runs of the modelling algorithm.

^b Scattering profiles up to $q_{max} = 2.6 \text{ nm}^{-1}$ and the parameters (R_G , V , M_M) for the atomic structures were calculated by the program CRY SOL with the radius of the atomic group $r_a = 0.160 \text{ nm}$ and the contrast of the hydration layer of $\delta\rho_b = 60 \text{ e nm}^{-3}$.

^c R_G value was obtained after extrapolation to infinite dilution; single values were calculated from Guinier fit using a q range of $0.14\text{--}0.3 \text{ nm}^{-1}$.

^d R_G and D_{max} values were calculated from the $p(r)$ function by the program GNOM.

^e R_{xs} value was calculated from the cross-sectional Guinier fit using a q range of $0.35\text{--}0.55 \text{ nm}^{-1}$.

^f Length of the particle $L = [12(R_G^2 - R_{xs}^2)]^{1/2}$.

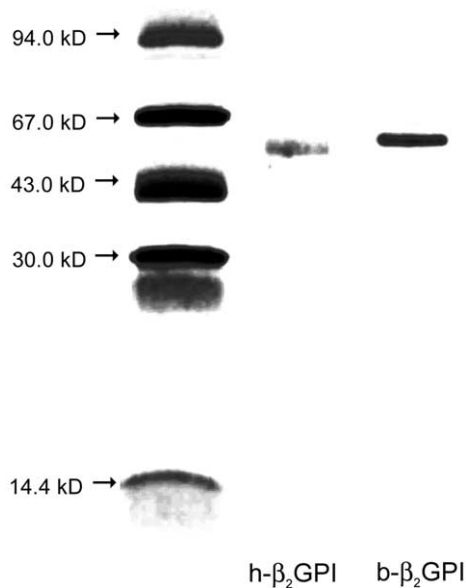


Figure 2. SDS-PAGE analysis of human β_2 GPI (lane 2) and bovine β_2 GPI (lane 3). A sample of protein (1 μ g) was applied to each lane (12.5% (w/v) polyacrylamide gel). Apparent molecular masses of 55.0 kDa for human β_2 GPI and 58.1 kDa for bovine β_2 GPI were determined. Lane 1: low molecular mass standard (Pharmacia).

Determination of low-resolution models for human and bovine β_2 GPI

Overall shape restoration from solution scattering data for human and bovine β_2 GPI was achieved by two different *ab initio* methods, namely DAMMIN²⁸ and DALAI_GA.²⁹ In both procedures, only SAXS profiles up to $q_{\max} = 2.6 \text{ nm}^{-1}$ for h- β_2 GPI and $q_{\max} = 3.2 \text{ nm}^{-1}$ for b- β_2 GPI were used for the fits. In DAMMIN, ten independent shape determinations were performed within a spherical search volume of $D_{\max} = 14.0 \text{ nm}$ for both proteins. The packing radius of the dummy atoms was 0.375 nm. The restored models for h- β_2 GPI yield $R_G = 4.26(\pm 0.01) \text{ nm}$, $D_{\max} = 13.4(\pm 0.05) \text{ nm}$ and $V = 105(\pm 2) \text{ nm}^3$ and display an S-like shape with a cross-section diameter of about 2 nm, as expected for a CCP domain (Figure 3(a)). The restored models for b- β_2 GPI have $R_G = 4.34(\pm 0.08) \text{ nm}$, $D_{\max} = 13.7(\pm 0.2) \text{ nm}$ and $V = 113(\pm 2) \text{ nm}^3$ (Figure 3(b)). The main structural features are depicted by superposition of five restored models with one template structure (Figure 3(c) and (d)). Despite differences in the structural details between the superimposed models, consistence was achieved in the location of side-arms, which are marked by arrows in the Figure. The side-arms most probably indicate the position of the N-linked carbohydrates attached to the protein.

In DALAI_GA, the same scattering profiles were used after manually subtracting a constant according to Porod's law for homogeneous particles in order to be consistent with DAMMIN, where this is done automatically. Ten independent

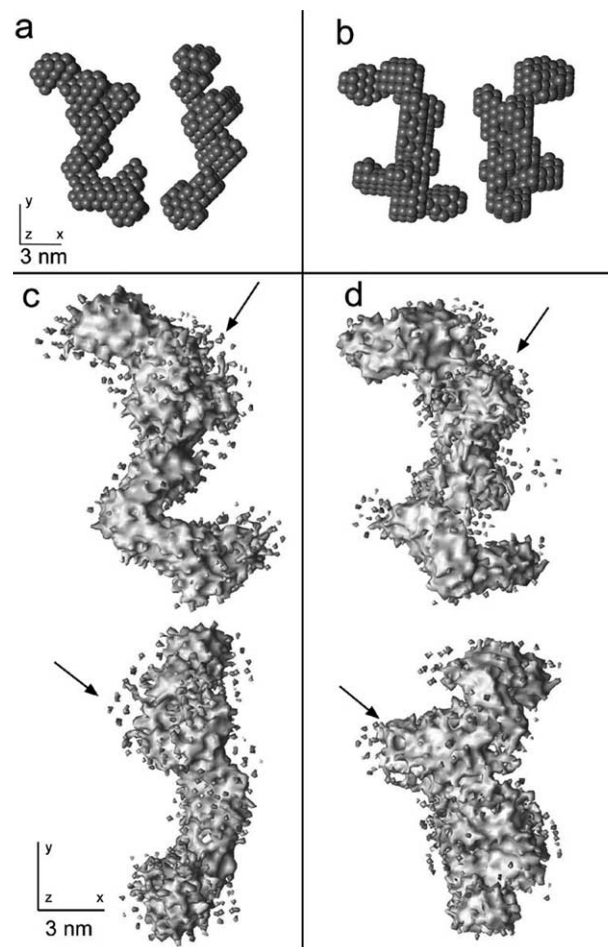


Figure 3. Low-resolution models restored by DAMMIN. Single restored models of (a) h- β_2 GPI and (b) b- β_2 GPI; on the right-hand side, the same model is presented rotated clockwise by 90° along the Y axis. Five superimposed different models of (c) h- β_2 GPI and (d) b- β_2 GPI are displayed in surface representation; the models at the bottom represent the same model rotated clockwise by 90° about the Y axis. The arrows mark the side-arms.

shape determinations were performed within an initial ellipsoidal search volume of $a = 15 \text{ nm}$, $b = c = 8 \text{ nm}$ for both proteins. The packing radius of the dummy beads was 0.4 nm. The restored models yielded $R_G = 4.21(\pm 0.03) \text{ nm}$, $D_{\max} = 13.3(\pm 0.1) \text{ nm}$ and $R_G = 4.25(\pm 0.06) \text{ nm}$, $D_{\max} = 13.9(\pm 0.5) \text{ nm}$, for h- β_2 GPI and b- β_2 GPI, respectively. A comparison with results from DAMMIN illustrates that the individual models from DALAI_GA are less packed, with more details and significantly reduced number of beads (Figure 4(a) and (b)). The observed differences in the compactness are caused by the fact that no connectivity restrictions during the shape determination were used. The reduced number of beads, which results in a smaller volume of the model, is caused by differences in the calculation of the scattering intensity by either the multiphase or the Debye formula.³⁰ However, the five superimposed models displayed in surface representation in Figure 4(c)

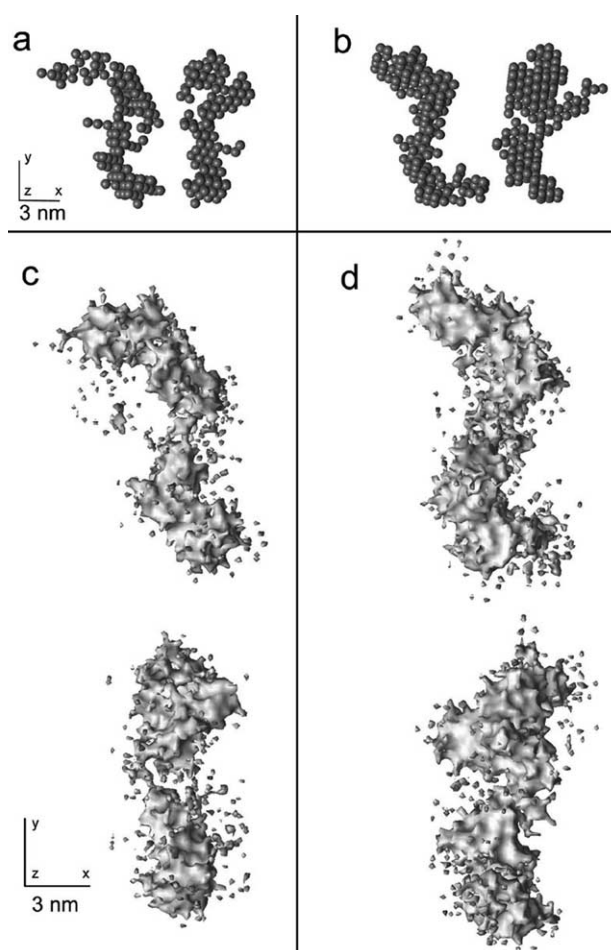


Figure 4. Low-resolution models restored by DALAI_GA. Single restored models of (a) h- β_2 GPI and (b) b- β_2 GPI; on the right-hand side, the same model is presented rotated clockwise by 90° about the Y axis. Five superimposed different models of (c) h- β_2 GPI and (d) b- β_2 GPI are displayed in surface representation; the models at the bottom represent the same model rotated clockwise by 90° about the Y axis.

and (d) reveal a remarkable similarity to the models restored by DAMMIN.

As already mentioned, only the low-resolution part of the scattering profile (low angles) was used to determine the shape of β_2 GPI. In order to include the higher-resolution part of the X-ray scattering pattern (up to $q_{\max} = 4.0 \text{ nm}^{-1}$) for structural modelling, the program GASBOR³¹ was used, applying the modifications that are necessary for a glycoprotein and are given in Materials and Methods. This program fits the experimental scattering profiles successfully, with r.m.s values of 0.013 ± 0.01 and 0.029 ± 0.02 for h- β_2 GPI and b- β_2 GPI, respectively. For better illustration, Figure 5(a) and (b) presents a model for both proteins as obtained by GASBOR shape determination. Again, the overall shapes of the single restored models are similar and resemble the models restored by DAMMIN and DALAI_GA, as shown in Figures 3 and 4, respectively. Note the similarity in the location of side-arms marked with arrows in

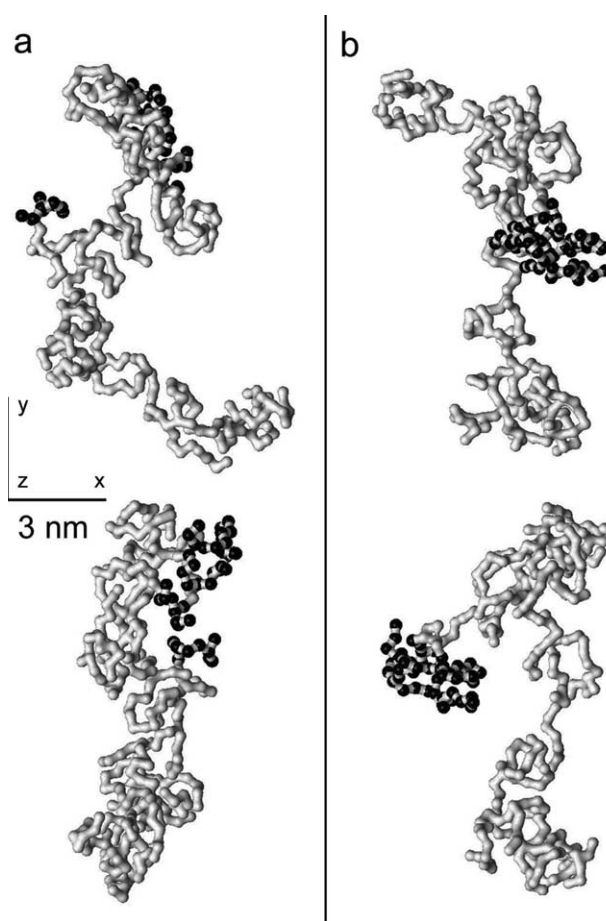


Figure 5. Single low-resolution models of (a) h- β_2 GPI and (b) b- β_2 GPI restored by GASBOR. The models at the bottom represent the same model rotated clockwise by 90° about the Y axis. The dark dots mark the side-arms.

Figure 3(b) and (c) and with dark dots in Figure 5(a) and (b).

Modification of the crystal structure of human β_2 GPI based on the low-resolution models

The theoretical SAXS profile and the $p(r)$ function calculated from the crystallographic coordinates of h- β_2 GPI (1C1Z.pdb) by the program CRY SOL³² are shown in Figure 6(a) and (b) (dotted lines). First, the discrepancy (r.m.s = 0.13) between the calculated and the experimental scattering profiles shows explicit differences. In general, the shapes of the $p(r)$ functions are typical for elongated particles. However, the $p(r)$ function calculated for the crystal structure shows a higher anisotropy in comparison to the $p(r)$ function obtained from solution experiments. The first maximum at $r = 1.9 \text{ nm}$ in the $p(r)$ function from the crystal structure correlates well with the cross-section value of the CCP domains. The maximum of the $p(r)$ functions from experimental data, however, is shifted to higher distances $r \sim 3.8 \text{ nm}$, whereas the first maximum at $r = 1.9 \text{ nm}$ is still preserved as a shoulder. These results indicate

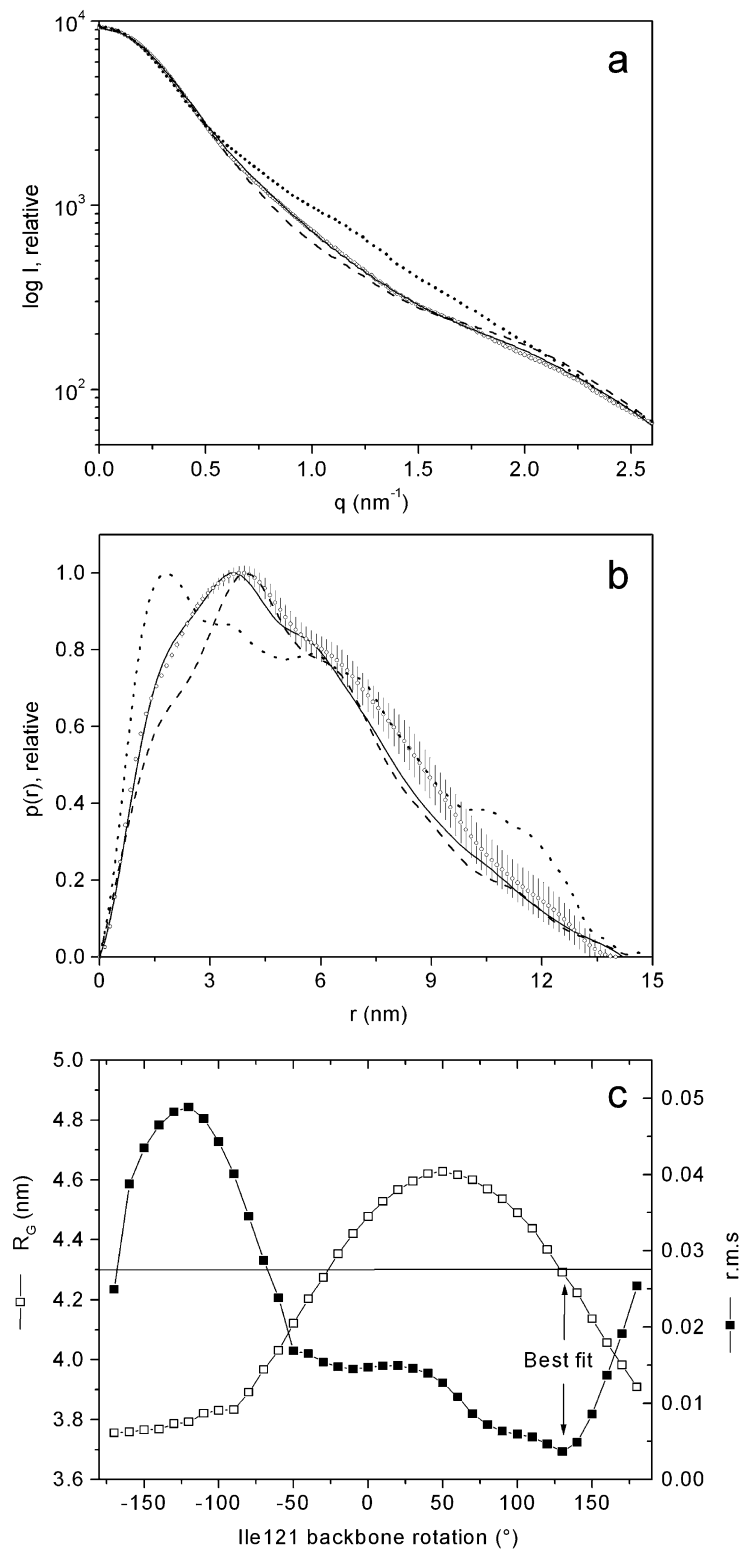


Figure 6. (a) The theoretical scattering profiles calculated from the crystal structure of h- β_2 GPI, PDB-code: 1C1Z (dotted line), the crystal structure modified by adding carbohydrate residues (broken line), 1C1Z modified by rotating the latter by 130° (continuous line) are fit to the experimental scattering profile of h- β_2 GPI (open circles). The theoretical scattering profiles were calculated with a radius of the atomic group $r_a = 0.160$ nm and a contrast of the hydration layer of $\delta\rho_b = 60$ e/nm³ by the program CRY SOL. (b) The corresponding distance distribution functions $p(r)$ calculated by the program GNOM. (c) R_G (\square) and r.m.s (\blacksquare) values calculated for 36 atomic models modified by rotation of the Ile121 backbone, where the rotation angle is incremented in 10° steps, whereas 0° rotation represents the crystal structure modified by adding carbohydrate residues. The straight line depicts the experimental R_G value, $R_G = 4.30$ nm.

that in comparison to the crystal structure the solution structure of h- β_2 GPI is more bulky but still elongated. Hence, it is essential to model the carbohydrate residues that are missing from the crystal structure. In particular, four carbohydrate chains were attached to the residual carbohydrate chains already detected in the crystal structure. The carbohydrate chains were modelled in differ-

ent folding states, whereas the unfolded chain with the highest solvent contact was determined as the configuration with the best fit (r.m.s = 0.015) (Figure 6(a), broken line). A higher value taken for the contrast of the hydration layer ($\delta\rho_b = 60$ e nm⁻³) results in a further slight improvement of the fit in the high q -range of the scattering curve. The corresponding $p(r)$ function for the

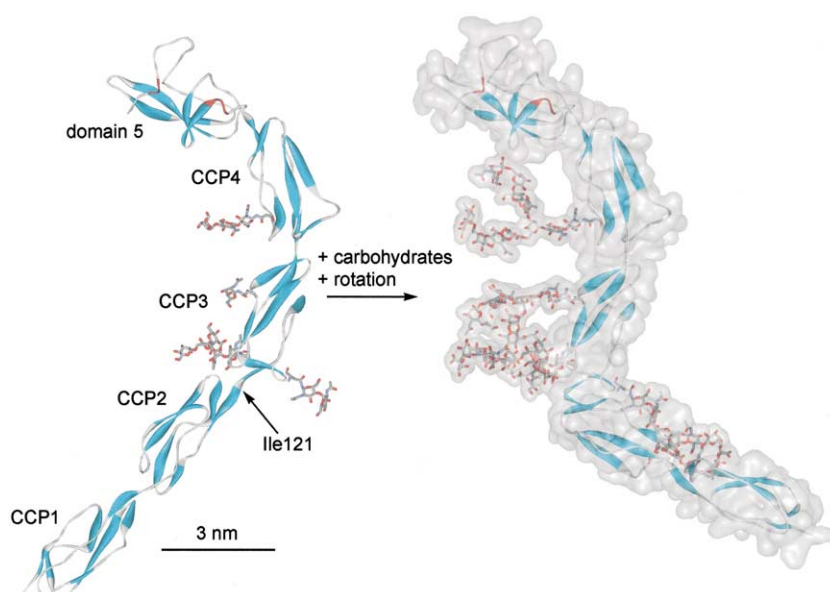


Figure 7. The crystal structure of h- β_2 GPI (left) is shown in comparison to the atomic model with complete carbohydrate chains and transformed according to the best fit to the experimental data (right). The secondary elements, β -strands and α -helix of the structure are shown as a continuous ribbon in blue and red, respectively. The four N-linked carbohydrates attached to the residues Asn143, Asn164, Asn174 and Asn234 drawn in all-atom mode are: -GlcNAc-GlcNAc-Man-(Man-GlcNAc-Gal-NeuAc)₂ (GlcNAc, N-acetylglucosamine; Man, mannose; Gal, galactose; NeuAc, N-acetylneuraminic acid \rightarrow sialic acid). The atomic model is additionally displayed in transparent surface presentation.

modified crystal structure with the added carbohydrates is displayed in Figure 6(b) (broken line). Although an improvement of the fit to the experimental data is achieved, a discrepancy for $q > 0.6 \text{ nm}^{-1}$ is observed. In this q -range, however, the influence of the scattering from the overall structure is still dominant. In order to improve the fit, one has to take into account the bending of the molecule. The differences in bending between the low-resolution models and the crystal structure most probably arise from different tilt and twist angles between the CCP domains. Accordingly, the crystal structure was rotated between domains CCP3 and CCP2, a region where remarkably little buried interface surface area was observed. The Ile121 backbone, where the β -strand of the domain linker shows a short random coil, was chosen as the most suitable rotation bond between CCP3 and CCP2. The R_G and r.m.s values calculated for 36 models, which differ in the rotation angle in the Ile121 backbone, are shown in Figure 6(c). The model with 0° rotation represents the modified crystal structure with added carbohydrate chains. The model with a rotation angle of 130° shows the best fit to the experimental profile (r.m.s = 0.004) and the calculated R_G value, $R_G = 4.29 \text{ nm}^{-1}$, is almost identical with the experimental value, $R_G = 4.30 \text{ nm}^{-1}$. The excellent fit of the calculated scattering profile for the model rotated by 130° to the experimental data as well as the almost identical $p(r)$ functions (Figure 6(a) and (b) continuous lines) are a clear indication for a different bending of h- β_2 GPI molecule in the crystal and in solution. The final model obtained by rotation (130°) displays an S-shaped structure (Figure 7) and closely resembles the low-resolution models. The tilt angle between CCP3 and CCP2 calculated for the structure with the best fit to the experimental SAXS data is $\sim 60^\circ$, whereas from the crystal structure an extremely low tilt angle of $\sim 20^\circ$ was

calculated. Additional evidence for the reliability of the solution structure determination arises from the fact that the calculated SAXS parameters (R_G , D_{max} , V) for the rotated model are in much better agreement with the experimental values (Table 1).

Table 1 shows the M_M values calculated from the crystal structure and from the models of h- β_2 GPI in comparison to the experimental data. The M_M calculated for the crystal structure including the carbohydrate chains is 45.7 kDa. This is considerably less than the M_M of 55.1 kDa estimated by SDS-PAGE, which may be higher in the case of glycoproteins.^{33,34}

Discussion

Differences between crystal and solution structure of human β_2 GPI

The experimental scattering profile fit poorly to the simulated curve calculated from the crystallographic coordinates of h- β_2 GPI. This fact, as well as the disagreements in the corresponding $p(r)$ functions, indicate differences in the overall shape of h- β_2 GPI in crystal and solution. From the SAXS parameters in Table 1, it is obvious that the solution structure is less elongated and more bulky. Due to the highly conserved structure of β_2 GPI subunits (CCP domains + domain V), changes in the overall shape can be attributed to different domain orientations only in the case of a monomeric solution. To obtain additional information, three *ab initio* modelling approaches were applied to fit the experimental scattering profile. The corresponding low-resolution solution structural models were restored. It should be noted that the single models presented here show variations between independent runs with similar goodness of fit and hence demonstrate that the SAXS shape

determination does not lead to unique solutions. However, the superimposed models display a consistent overall structure, which confirms that the information content in the scattering profiles justifies the *ab initio* modeling. Further, it should be stressed that the models obtained by GASBOR (Figure 5), although they display the location of C^α atoms, are of low resolution, i.e. 1.6 nm, which is defined by the range of data fitting. However, it was possible to distinguish between main structural features and side-arms. The side-arms in the models can be attributed to the carbohydrate units attached to the asparagine residues 164, 174, and 234. These three carbohydrate units are in close vicinity to each other, which results in a bulky structural feature seen by SAXS. After attaching the missing carbohydrates to the crystal structure, a significant improvement in the fit of the calculated scattering profile as well as of the $p(r)$ function of h- β_2 GPI to the experimental data was achieved (Figure 6(a) and (b)). However, we considered the fit not sufficiently good. Accordingly, the J-shaped crystal structure was modified, applying a rotation at the most suitable interdomain linker bond (Ile121) (Figure 7). The analysis of various models rotated in increments of 10° revealed that, in agreement with the low-resolution models, an S-shaped structure shows the best fit to the experimental data. This model yields a tilt angle of $\sim 60^\circ$ between CCP3 and CCP2, which is in disagreement with the $\sim 20^\circ$ calculated from the crystal structure. Low tilt angles of $\sim 20^\circ$ are extremely rare,³⁵ whereas tilt angles of $\sim 60^\circ$ are likely to be a common structural feature in proteins with CCP domains, e.g. in human factor H (HFH 15–16 = $50(\pm 13)^\circ$),³⁶ measles virus binding protein (CD46 1–2 = $60(\pm 15)^\circ$),³⁷ vaccinia virus protein (VCP 3–4 = $59(\pm 4)^\circ$)³⁸ and in β_2 GPI between CCP3–CCP4 ($\sim 60^\circ$).

In conclusion, it can be postulated that under nearly physiological conditions, β_2 GPI is more bent and forms an averaged S-shaped solution structure despite domain oscillations. However, the exact characterization of the domain orientation in a system of five domains connected with four flexible linkers is not reasonable. A potential reason for an overall shape of h- β_2 GPI different from the crystal structure might be the very high ionic strength used during the crystallization procedure ($I = 6$ M). High ionic strength destabilizes the interdomain hydrogen bonds and, accordingly, the crystal packing is dominated mainly by intermolecular hydrophobic interactions involving CCP1, CCP2 and domain V, resulting in a J-shape. The results presented here for h- β_2 GPI suggest that crystallization conditions as well as the crystal packing forces might affect the orientation of protein subunits in the crystal.

Differences between human and bovine β_2 GPI

In view of the scattering profiles and the $p(r)$ functions shown in Figure 1, an overall shape simi-

larity between b- β_2 GPI and h- β_2 GPI is obvious. Further evidence for a similar tertiary structure is given by the 83% homology in the amino acid sequence and the four characteristic CCP domains with identical numbers of disulfide bonds followed by one lipid-binding domain.³⁹ However, in the present work, the small increase of size in the experimental and model parameters for b- β_2 GPI compared to h- β_2 GPI (Table 1) indicates a more bulky shape of b- β_2 GPI. These results are in good agreement with data from SDS–PAGE (Figure 2) in which the molecular mass for b- β_2 GPI was about 3 kDa higher compared to h- β_2 GPI, probably caused by an additional Asn73 N-linked carbohydrate.³⁹ To summarize, the restored low-resolution models of b- β_2 GPI displayed a similar S-shape with less bending in the central part.

Functional implication

The structure of β_2 GPI in solution as presented here exhibits a well defined spatial orientation and, due to the flexibility of the interdomain linkers, can adopt an optimal spatial and entropic conformation through bending. However, the structure is not necessarily conserved. For example, in other cases, like in factor H, which is composed of 20 CCP domains, the solution structure exhibits a mixture of different domain orientations driven by the fact that five longer linkers (up to eight amino acid residues each) permit a positional variation of the overall structure.⁴⁰ Thus, proteins consisting of CCP or similar domains can adopt different conformations, where the variations depend critically on the flexibility and length of the linkers and on certain spatial restrictions.^{41,42}

The solution structure determined for β_2 GPI under nearly physiological conditions can put into perspective different hypotheses for interaction of β_2 GPI with membranes or aPLAs. In the literature, some studies stress that binding of β_2 GPI to acidic phospholipids alters the secondary structure of the protein slightly, thus exposing autoepitopes,^{21,25} whereas others advocate that dimerisation or clustering of β_2 GPI^{43,44} is essential for bivalent binding of aPLAs.^{45,46} Only recently, it was shown that dimeric chimeras of β_2 GPI have a much higher affinity for phospholipids.²⁴ From this point of view, the solution structure represents the free, not immobilized structure, which is described as immunologically less active.²⁶ It is conceivable that transitions between conformational states directly correlate with the functional activity of the protein. Immobilisation or cross-reacting of β_2 GPI domains due to ligand binding²² may cause the exposure of cryptic epitopes^{19–21,47} and reorientations of CCP-domains, probably required for aPLAs interaction. If so, this “bending” and “stretching” of the β_2 GPI molecule could provide a mechanism for its biological control.

Despite the limited resolution, SAXS is certainly a useful tool to investigate the tertiary structure of complex proteins in solution. This is of great importance as the solution structure is sensitive to conformational changes, which are fundamental for the physiological role of a protein. In our case, the structures of the glycoprotein obtained by X-ray crystallography and solution scattering are quite different. With the help of SAXS measurements, we could model carbohydrate residues that are not resolved in the crystal structure. By analogy, this method could be applied to predict the spatial orientation of a homologous structure that has not been solved by X-ray crystallography.

Materials and Methods

Protein isolation and purification

β_2 GPI was isolated from citrated human or bovine plasma as described.^{1,48} In brief, the protein was purified by affinity column chromatography, dialysed exhaustively against Tris-HCl (pH 7.4) and finally dialysed against NH_4HCO_3 before lyophilization. The preparation was virtually 100% pure as judged by SDS-PAGE, yielding a single band with an apparent molecular mass of 55.0 kDa for h- β_2 GPI and 58.1 kDa for b- β_2 GPI. The protein was dissolved in 50 mM Tris-HCl (pH 7.4), 25 mM NaCl before use. The protein concentration was measured by the bicinchoninic acid assay (BCA assay, Pierce, The Netherlands).

Small-angle X-ray scattering

Measurements were carried out using a Kratky compact camera (Hecus MBraun, Graz, Austria),⁴⁹ equipped with a thermostatically controlled sample holder. The measurements were performed at 20 °C using a quartz capillary with a volume of 60 μl and an inner diameter of 1.0 mm. Protein concentrations of 5, 10, 20, and 30 mg/ml were used. A Ni-filtered primary X-ray beam was generated by a water-cooled rotating Cu-anode generator (Rigaku Corp., Japan). The sample to detector distance was 272 mm and the position calibration of the detector was performed using Ag-stearate as a standard. Scattering curves were monitored in a q -range from 0.14 to 4.0 nm^{-1} ($q = 4\pi\sin\theta/\lambda$), with 2θ being the scattering angle and $\lambda = 0.15418$ nm (Cu K α radiation) being the wavelength of the X-ray. Exposure times were typically 3600 seconds for individual measurements. The scattering of the buffer was subtracted after absorption correction and the difference scattering curve was normalized to a concentration of 1 mg/ml. The normalized curves were extrapolated to zero concentration using standard procedures.⁵⁰ The final composite scattering curve was obtained by merging the low-angle data ($0.14 < q < 0.8$ nm^{-1}) extrapolated to zero concentration with the high-angle data ($0.8 < q < 4.0$ nm^{-1}) recorded at a high concentration (30 mg/ml). The resulting scattering data were subjected to indirect Fourier transformation using the program GNOM,⁵¹ which performs a desmearing of the raw data with the slit-width, and slit length, profiles of the primary beam from the slit collimation. Radii of gyration (R_G) were further determined by Guinier approximation from the low q -regions

of the scattering profiles, yielding also the scattering intensity extrapolated to the zero angle $I(0)$:⁵⁰

$$\ln I(q) = \ln I(0) - R_G^2 q^2 / 3 \quad (1)$$

$I(0)$ on a relative intensity scale was used to calculate the molecular mass (M_M) of β_2 GPI using lysozyme with a known M_M of 14.4 kDa as a reference.^{52,53} For elongated particles, the mean radius of gyration of the cross-section R_{xs} and the mean cross-sectional intensity at zero angle $[I(q)q]_{q \rightarrow 0}$ is obtained from:

$$\ln[I(q)q] = \ln[I(q)q]_{q \rightarrow 0} - R_{xs}^2 q^2 / 2 \quad (2)$$

R_G and R_{xs} were used to analyze the triaxial dimensions of β_2 GPI where the length of the particle is $L = [12(R_G^2 - R_{xs}^2)]^{1/2}$. For an elongated particle, $L \approx D_{\max}$ can be assumed. The scattering profiles in the range up to $q_{\max} = 4.0$ nm^{-1} were used to compute the volumes V of the hydrated particles.⁵⁰ $V = 2\pi^2(I(0)/Q)$, where Q is the invariant according to Porod.⁵⁴ The program GNOM was used to compute the pair-distance distribution function $p(r)$, which represents the probability of finding a point within the particle at a distance r from a given point. Integrating this probability over the surface of the sphere of radius R and over the volume V yields the $p(r)$ function as expressed by:

$$p(r) = \frac{1}{2\pi^2} \int_0^\infty r q I(q) \sin(rq) dq \quad (3)$$

This offers an alternative calculation of R_G and $I(0)$ that is based on the full scattering curve,⁵⁰ and gives the maximum dimension of the macromolecule D_{\max} , as the distance where the $p(r)$ function approaches zero.

Ab initio deconvolution of the SAXS profile

The low-resolution shapes of β_2 GPI were restored from the experimental data by two independent *ab initio* shape-determination programs, DAMMIN²⁸ and DALAI_GA.²⁹ Scattering profiles up to $q_{\max} = 2.6$ nm^{-1} for human and $q_{\max} = 3.2$ nm^{-1} for bovine β_2 GPI were used for the fit. DAMMIN calculates the scattering intensities from a multiphase model of a particle built up from a finite number of dummy beads that are characterized by the configuration vector assigning the beads to a specific phase or to the solvent. DALAI_GA calculates the scattering intensities of a given molecular structure defined by dummy beads (assuming the homogeneous electron density) according to the Debye formula.⁵⁵ More detailed information about the approaches used for the calculation of scattering intensity from beads models can be found in the literature.^{28,29} Each method starts searching for a model in a volume filled by uniformly hexagonally packed beads with dimensions selected according to the resolution of the scattering profile and taking into account the dimension of the initial search object. DAMMIN searches for the best model configuration, minimizing the discrepancy function:

$$f(X) = \chi^2 + \alpha P(X) \quad (4)$$

between the calculated and experimental curves using the simulated annealing method.⁵⁶ Here, χ is the discrepancy between calculated and experimental curve, and $\alpha P(X)$ is a looseness penalty with positive weight $\alpha > 0$. The idea of this method is to modify the coordinates of beads randomly, while always approaching the configurations that decrease the energy $f(X)$. DALAI_GA uses a genetic algorithm⁵⁷ for iterative fitting of the

scattering profile. In this approach, the initial model population is generated randomly, within some restrictions, and for each model a fitness value:

$$F = \left(\sum_i (\log(I_{\text{exp}}(q_i)) - \log(I_{\text{model}}(q_i)))^2 \right)^{-1/2} \quad (5)$$

is assigned. The models are combined using genetic operators in such a way that the better fits have a higher probability of “reproducing”. The repeated genetic operators to the fittest models increase the average fitness of the population. This process is repeated until the system converges or a good enough model is found.

To improve the resolution and reliability of models, an additional *ab initio* modelling approach, GASBOR was used.³¹ This procedure fits the scattering profiles up to $q_{\text{max}} = 4.0 \text{ nm}^{-1}$ and hence shows the highest resolution for the β_2 GPI models ($2\pi/q_{\text{max}} = 1.6 \text{ nm}$). GASBOR uses a simulated annealing approach to find a chain-compatible spatial distribution of an exact number of dummy residues that corresponds to the distribution of C^α atoms of amino acid residues. The calculation of the scattering intensity from the model is based on the Debye formula.⁵⁵ In this fitting approach, the numbers of amino acid residues of the protein have to be specified. In the case of a glycoprotein, the contribution of the scattering from carbohydrates has to be taken into account. Due to different mean electron densities ($\bar{\rho}$) of carbohydrates and proteins, the number of carbohydrate residues has to be adjusted the following way in order to be counted as amino acid residues

$$N_{\text{residues}} = N_{\text{carbohydrate residues}}(\bar{\rho}_{\text{carbohydrate}} - \bar{\rho}_{\text{buffer}}) / (\bar{\rho}_{\text{protein}} - \bar{\rho}_{\text{buffer}}) \quad (6)$$

where N_{residues} and $N_{\text{carbohydrate residues}}$ are the numbers of amino acid residues and carbohydrate residues, respectively. $\bar{\rho}$ of protein and buffer were set to $\bar{\rho}_{\text{protein}} = 447 \text{ e nm}^{-3}$ and $\bar{\rho}_{\text{buffer}} = 334.5 \text{ e nm}^{-3}$, respectively.⁵⁸ The ρ of carbohydrates can be calculated from \bar{z} (electron concentration in e g^{-1}) and the partial specific volume (v_2), according to

$$\bar{\rho} = \bar{z}(v_2)^{-1} N_A \times 10^{-21}. \quad (7)$$

In particular, human β_2 GPI has four N-linked carbohydrate units attached to the Asn residues 143, 164, 174, 234^{9,10} (see the legend to Figure 7). Bovine β_2 GPI shows glycosylation sites identical with that of an additional site located on Asn73.⁵⁹ According to the deglycosylated derivatives⁶⁰ prepared enzymatically, a similarity between all carbohydrate units with a complex type can be assumed. Nevertheless, the possibility of a slight heterogeneity in sialylation cannot be excluded.⁶¹ The electron concentration $\bar{z} = 0.534 \text{ e g}^{-1}$ and the partial specific volume $v_2 = 0.63 \text{ cm}^3 \text{ g}^{-1}$ ⁶² for the carbohydrate units give the mean electron density of $\bar{\rho}_{\text{carbohydrate}} = 510.4 \text{ e nm}^{-3}$. Applying equation (6), the 44 and 55 carbohydrate residues located in four h- β_2 GPI and five b- β_2 GPI carbohydrate chains consequently correspond to 69 and 86 amino acid residues, respectively.

The goodness of fit for all three above-mentioned *ab initio* methods was measured using the root mean square

deviation (r.m.s) for N intensities $I(q)$ according to:

$$\text{r.m.s} = \left(\sum_i^N (\log(I_{\text{exp}}(q_i)) - \log(I_{\text{model}}(q_i)))^2 / N^{-2} \right) \quad (8)$$

Application of theoretical SAXS profiles in crystal structure modification

The crystallographic coordinates with PDB-code 1C1Z⁹ were used as an atomic model of human β_2 GPI. The theoretical scattering curve from the crystal structure was calculated using the program CRY SOL,³² which surrounds the macromolecule by a 0.3 nm thick hydration layer with a slightly greater electron density than the solvent.⁶³ The final scattering intensity is calculated as the addition of scattering of the particle in vacuum and the hydration layer followed by subtraction of scattering from the excluded volume. The program either calculates the scattering profile or fits the experimental data whenever the average excluded volume per atomic group r_a and the contrast of the hydration layer $\delta\rho_b$ are adjustable parameters to minimize the discrepancy between experimental and calculated curves. This fitting approach was used to match the modifications done within the crystal structure to the experimental scattering profile. Structural modifications include rotation of CCP domains and attachment of sugar units. The modifications were carried out using the program WebLabViewerPro 4.0 (Accelrys Inc.).

Domain orientation

Domain orientations, specified by tilt angles, have been evaluated for crystal and atomic models as follows. For the CCP1 domain, the inertia tensor was calculated and diagonalised. The main unitary vectors z with origin in the center of mass were aligned along the major axes of the inertia tensor. CCP domains 2–4 and domain V were superimposed with CCP1. Superposition of the CCP domains was performed by the program SUPCOMB⁶⁴ using C^α positions of spatially related residues. The related unitary vectors z' for each domain were calculated from the transformation matrix obtained by superimposing procedures. The tilt angle ε between neighbor domains is given by the angle $\cos(\varepsilon) = zz'$ calculated for the neighbour domains. Definition of the tilt angle ε is according to Bork *et al.*³⁵

Acknowledgments

We thank Sarah Tutz, Margit Eichholzer and Josef Kellner for excellent technical assistance. We greatly appreciate Robert Schwarzenbacher's constructive comments. This work was supported by a grant from the Austrian Science Foundation (Project P13872-CHE to R.P.).

References

- Polz, E. & Kostner, G. M. (1979). Binding of beta 2-glycoprotein-I to intralipid: determination of the dissociation constant. *Biochem. Biophys. Res. Commun.* **90**, 1305–1312.

2. Wurm, H. (1984). Beta-2-glycoprotein-I (apolipoprotein-H) interactions with phospholipid-vesicles. *Int. J. Biochem.* **16**, 511–515.
3. Brighton, T. A., Hogg, P. J., Dai, Y. P., Murray, B. H., Chong, B. H. & Chesterman, C. N. (1996). Beta 2-glycoprotein I in thrombosis: evidence for a role as a natural anticoagulant. *Br. J. Haematol.* **93**, 185–194.
4. Nimpf, J., Bevers, E. M., Bomans, P. H., Till, U., Wurm, H., Kostner, G. M. & Zwaal, R. F. (1986). Prothrombinase activity of human platelets is inhibited by beta 2-glycoprotein-I. *Biochim. Biophys. Acta*, **884**, 142–149.
5. Shi, W., Chong, B. H., Hogg, P. J. & Chesterman, C. N. (1993). Anticardiolipin antibodies block the inhibition by beta 2-glycoprotein I of the factor Xa generating activity of platelets. *Thromb. Haemostasis*, **70**, 342–345.
6. Field, S. L., Brighton, T. A., McNeil, H. P. & Chesterman, C. N. (1999). Recent insights into anti-phospholipid antibody-mediated thrombosis. *Bailliere's Best Pract. Res. Clin. Haematol.* **12**, 407–422.
7. Kristensen, T., Schousboe, I., Boel, E., Mulvihill, E. M., Hansen, R. R., Moller, K. B. *et al.* (1991). Molecular-cloning and mammalian expression of human beta-2-glycoprotein-I cDNA. *FEBS Letters*, **289**, 183–186.
8. Steinkasserer, A., Estaller, C., Weiss, E. H., Sim, R. B. & Day, A. J. (1991). Complete nucleotide and deduced amino-acid-sequence of human beta-2-glycoprotein-I. *Biochem. J.* **277**, 387–391.
9. Schwarzenbacher, R., Zeth, K., Diederichs, K., Gries, A., Kostner, G. M., Laggner, P. & Prassl, R. (1999). Crystal structure of human beta2-glycoprotein I: implications for phospholipid binding and the anti-phospholipid syndrome. *EMBO J.* **18**, 6228–6239.
10. Bouma, B., de Groot, P. G., van Den Elsen, J. M., Ravelli, R. B., Schouten, A., Simmelink, M. J. *et al.* (1999). Adhesion mechanism of human beta(2)-glycoprotein I to phospholipids based on its crystal structure. *EMBO J.* **18**, 5166–5174.
11. Schousboe, I. (1988). Inositolphospholipid-accelerated activation of prekallikrein by activated factor-XII and its inhibition by beta-2-glycoprotein-I. *Eur. J. Biochem.* **176**, 629–636.
12. Delpapa, N., Sheng, Y. H., Raschi, E., Kandiah, D. A., Tincani, A., Khamashta, M. A. *et al.* (1998). Human beta 2-glycoprotein I binds to endothelial cells through a cluster of lysine residues that are critical for anionic phospholipid binding and offers epitopes for anti-beta 2-glycoprotein I antibodies. *J. Immunol.* **160**, 5572–5578.
13. Balasubramanian, K. & Schroit, A. J. (1998). Characterization of phosphatidylserine-dependent beta(2)-glycoprotein I macrophage interactions—implications for apoptotic cell clearance by phagocytes. *J. Biol. Chem.* **273**, 29272–29277.
14. McNeil, H. P., Simpson, R. J., Chesterman, C. N. & Krilis, S. A. (1990). Anti-phospholipid antibodies are directed against a complex antigen that includes a lipid-binding inhibitor of coagulation: beta 2-glycoprotein I (apolipoprotein H). *Proc. Natl Acad. Sci. USA*, **87**, 4120–4124.
15. Guerin, J., Feighery, C., Sim, R. B. & Jackson, J. (1997). Antibodies to beta(2)-glycoprotein I—a specific marker for the antiphospholipid syndrome. *Clin. Expt. Immunol.* **109**, 304–309.
16. Gharavi, A. E., Cucurull, E., Tang, H., Silver, R. M. & Branch, D. W. (1998). Effect of antiphospholipid antibodies on beta(2)glycoprotein I—phospholipid interaction. *Am. J. Reprod. Immunol.* **39**, 310–315.
17. Steinkasserer, A., Barlow, P. N., Willis, A. C., Kertesz, Z., Campbell, I. D., Sim, R. B. & Norman, D. G. (1992). Activity, disulfide mapping and structural modeling of the fifth domain of human-beta-2-glycoprotein-I. *FEBS Letters*, **313**, 193–197.
18. Hoshino, M., Hagihara, Y., Nishii, I., Yamazaki, T., Kato, H. & Goto, Y. (1998). Identification of the phospholipid-binding site of human beta(2)-glycoprotein I domain V by heteronuclear magnetic resonance. *J. Mol. Biol.* **304**, 927–939.
19. George, J., Gilburd, B., Hojnik, M., Levy, Y., Langevitz, P., Matsuura, E. *et al.* (1998). Target recognition of beta(2)-glycoprotein I (beta(2)GPI)-dependent anticardiolipin antibodies: evidence for involvement of the fourth domain of beta(2)GPI in antibody binding. *J. Immunol.* **160**, 3917–3923.
20. Iverson, G. M., Victoria, E. J. & Marquis, D. M. (1998). Anti-beta2 glycoprotein I (beta2GPI) autoantibodies recognize an epitope on the first domain of beta2GPI. *Proc. Natl Acad. Sci. USA*, **95**, 15542–15546.
21. Matsuura, E., Inagaki, J., Kasahara, H., Yamamoto, D., Atsumi, T., Kobayashi, K. *et al.* (2000). Proteolytic cleavage of beta(2)-glycoprotein I: reduction of antigenicity and the structural relationship. *Int. Immunol.* **12**, 1183–1192.
22. Hammel, M., Schwarzenbacher, R., Gries, A., Kostner, G. M., Laggner, P. & Prassl, R. (2001). Mechanism of the interaction of beta(2)-glycoprotein I with negatively charged phospholipid membranes. *Biochemistry*, **40**, 14173–14181.
23. Hagihara, Y., Hong, D. P., Hoshino, M., Enjyoji, K., Kato, H. & Goto, Y. (2002). Aggregation of beta(2)-glycoprotein I induced by sodium lauryl sulfate and lysophospholipids. *Biochemistry*, **41**, 1020–1026.
24. Lutters, B. C., Meijers, J. C., Derksen, R. H., Arnout, J. & de Groot, P. G. (2001). Dimers of beta 2-glycoprotein I mimic the *in vitro* effects of beta 2-glycoprotein I-anti-beta 2-glycoprotein I antibody complexes. *J. Biol. Chem.* **276**, 3060–3067.
25. Wang, S. X., Sun, Y. T. & Sui, S. F. (2000). Membrane-induced conformational change in human apolipoprotein H. *Biochem. J.* **348**, 103–106.
26. Keeling, D. M., Wilson, A. J., Mackie, I. J., Machin, S. J. & Isenberg, D. A. (1992). Some antiphospholipid antibodies bind to beta 2-glycoprotein I in the absence of phospholipid. *Br. J. Haematol.* **82**, 571–574.
27. Svergun, D. I., Malfois, M., Koch, M. H., Wigneshweraraj, S. R. & Buck, M. (2000). Low resolution structure of the sigma54 transcription factor revealed by X-ray solution scattering. *J. Biol. Chem.* **275**, 4210–4214.
28. Svergun, D. I. (1999). Restoring low resolution structure of biological macromolecules from solution scattering using simulated annealing. *Biophys. J.* **76**, 2879–2886.
29. Chacon, P., Moran, F., Diaz, J. F., Pantos, E. & Andreu, J. M. (1998). Low-resolution structures of proteins in solution retrieved from X-ray-scattering with a genetic algorithm. *Biophys. J.* **74**, 2760–2775.
30. Chacon, P., Diaz, J. F., Moran, F. & Andreu, J. M. (2000). Reconstruction of protein form with X-ray solution scattering and a genetic algorithm. *J. Mol. Biol.* **299**, 1289–1302.
31. Svergun, D. I., Petoukhov, M. V. & Koch, M. H. (2001). Determination of domain structure of

- proteins from X-ray solution scattering. *Biophys. J.* **80**, 2946–2953.
32. Svergun, D., Barberato, C. & Koch, M. H. J. (1995). CRY SOL—a program to evaluate X-ray solution scattering of biological macromolecules from atomic coordinates. *J. Appl. Crystallog.* **28**, 768–773.
 33. Leonard, C. K., Spellman, M. W., Riddle, L., Harris, R. J., Thomas, J. N. & Gregory, T. J. (1990). Assignment of intrachain disulfide bonds and characterization of potential glycosylation sites of the type 1 recombinant human immunodeficiency virus envelope glycoprotein (gp120) expressed in Chinese hamster ovary cells. *J. Biol. Chem.* **265**, 10373–10382.
 34. Pennica, D., Kohr, W. J., Fendly, B. M., Shire, S. J., Raab, H. E., Borhardt, P. E. *et al.* (1992). Characterization of a recombinant extracellular domain of the type 1 tumor necrosis factor receptor: evidence for tumor necrosis factor- α induced receptor aggregation. *Biochemistry*, **31**, 1134–1141.
 35. Bork, P., Downing, A. K., Kieffer, B. & Campbell, I. D. (1996). Structure and distribution of modules in extracellular proteins. *Quart. Rev. Biophys.* **29**, 119–167.
 36. Barlow, P. N., Steinkasserer, A., Norman, D. G., Kieffer, B., Wiles, A. P., Sim, R. B. & Campbell, I. D. (1993). Solution structure of a pair of complement modules by nuclear magnetic resonance. *J. Mol. Biol.* **232**, 268–284.
 37. Casanovas, J. M., Larvie, M. & Stehle, T. (1999). Crystal structure of two CD46 domains reveals an extended measles virus-binding surface. *EMBO J.* **18**, 2911–2922.
 38. Wiles, A. P., Shaw, G., Bright, J., Perczel, A., Campbell, I. D. & Barlow, P. N. (1997). NMR studies of a viral protein that mimics the regulators of complement activation. *J. Mol. Biol.* **272**, 253–265.
 39. Kato, H. & Enjyoji, K. (1991). Amino acid sequence and location of the disulfide bonds in bovine beta 2 glycoprotein I: the presence of five Sushi domains. *Biochemistry*, **30**, 11687–11694.
 40. Aslam, M. & Perkins, S. J. (2001). Folded-back solution structure of monomeric factor H of human complement by synchrotron X-ray and neutron scattering, analytical ultracentrifugation and constrained molecular modelling. *J. Mol. Biol.* **309**, 1117–1138.
 41. Kirkitadze, M. D., Dryden, D. T., Kelly, S. M., Price, N. C., Wang, X., Krych, M. *et al.* (1999). Co-operativity between modules within a C3b-binding site of complement receptor type 1. *FEBS Letters*, **459**, 133–138.
 42. Copie, V., Tomita, Y., Akiyama, S. K., Aota, S., Yamada, K. M., Venable, R. M. *et al.* (1998). Solution structure and dynamics of linked cell attachment modules of mouse fibronectin containing the RGD and synergy regions: comparison with the human fibronectin crystal structure. *J. Mol. Biol.* **277**, 663–682.
 43. Sheng, Y. H., Kandiah, D. A. & Krilis, S. A. (1998). Anti-beta(2)-glycoprotein I autoantibodies from patients with the antiphospholipid syndrome bind to beta(2)-glycoprotein I with low affinity: dimerization of beta(2)-glycoprotein I induces a significant increase in anti-beta(2)-glycoprotein I antibody affinity. *J. Immunol.* **161**, 2038–2043.
 44. Galazka, M., Tang, M., Debari, V. A., Kohles, J. D., Lee, J. K., Keil, L. B. & Petersheim, M. (1999). Modification of beta(2)glycoprotein I by glutardialdehyde—conformational changes and aggregation accompany exposure of the cryptic autoepitope. *Appl. Biochem. Biotech.* **76**, 1–13.
 45. Roubey, R. A. S., Eisenberg, R. A., Harper, M. F. & Winfield, J. B. (1995). Anticardiolipin autoantibodies recognize b2-glycoprotein I in the absence of phospholipid. *J. Immunol.*, 954–960.
 46. Willems, G. M., Janssen, M. P., Pelsers, M. A. L., Comfurius, P., Galli, M., Zwaal, R. F. A. & Bevers, E. M. (1996). Role of divalency in the high-affinity binding of anticardiolipin antibody-beta(2)-glycoprotein-I complexes to lipid-membranes. *Biochemistry*, **35**, 13833–13842.
 47. Hasunuma, Y., Matsuura, E., Makita, Z., Katahira, T., Nishi, S. & Koike, T. (1997). Involvement of beta(2)-glycoprotein-I and anticardiolipin antibodies in oxidatively modified low-density-lipoprotein uptake by macrophages. *Clin. Expt. Immunol.* **107**, 569–573.
 48. Gries, A., Nimpf, J., Wurm, H., Kostner, G. M. & Kenner, T. (1989). Characterization of isoelectric subspecies of asialo-beta 2-glycoprotein I. *Biochem. J.* **260**, 531–534.
 49. Laggner, P. & Mio, H. (1992). SWAX—a dual-detector camera for simultaneous small- and wide-angle X-ray diffraction in polymer and liquid crystal research. *Nucl. Instrum. Method A*, **323**, 86–90.
 50. Glatter, O. (1982). Data treatment. In *Small Angle X-ray Scattering* (Glatter, O. & Kratky, O., eds), pp. 119–166, Academic Press, London.
 51. Svergun, D. I. (1992). Determination of the regularization parameter in indirect-transform methods using perceptual criteria. *J. Appl. Crystallog.* **25**, 495–503.
 52. Kratky, O. (1963). X-ray small angle scattering with substances of biological interest in diluted solutions. *Prog. Biophys. Chem.* **13**, 105–173.
 53. Wignall, G. D. & Bates, F. S. (1987). Absolute calibration of small angle neutron scattering data. *J. Appl. Cryst.* **20**, 28–40.
 54. Porod, (1982). General theory. In *Small Angle X-ray Scattering* (Glatter, O. & Kratky, O., eds), pp. 17–51, Academic Press, London.
 55. Debye, P. (1915). Zerstreuung von Röntgenstrahlen. *Ann. Phys.* **46**, 809–823.
 56. Kirkpatrick, S., Gelatt, C. D., Jr. & Vecchi, M. P. (1983). Optimization by simulated annealing. *Science*, **220**, 671–680.
 57. Goldberg, D. E. (1989). *Genetics Algorithms in Search, Optimisation and Machine Learning*, Addison-Wesley, San Mateo, CA.
 58. Müller, K., Laggner, P., Glatter, O. & Kostner, G. M. (1978). The structure of human-plasma low-density lipoprotein B. *Eur. J. Biochem.* **82**, 73–90.
 59. Bendixen, E., Halkier, T., Magnusson, S., Sottrup-Jensen, L. & Kristensen, T. (1992). Complete primary structure of bovine beta 2-glycoprotein I: localization of the disulfide bridges. *Biochemistry*, **31**, 3611–3617.
 60. Walsh, M. T., Watzlawick, H., Putnam, F. W., Schmid, K. & Brossmer, R. (1990). Effect of the carbohydrate moiety on the secondary structure of beta-2-glycoprotein. 1. Implications for the biosynthesis and folding of glycoproteins. *Biochemistry*, **29**, 6250–6257.
 61. Kornfeld, R. & Kornfeld, S. (1976). Comparative aspects of glycoprotein structure. *Annu. Rev. Biochem.* **45**, 217–237.

-
62. Charlwood, P. (1957). Partial specific volumes of proteins in relation to composition and environment. *J. Am. Chem. Soc.* **79**, 776–781.
63. Svergun, D. I., Richard, S., Koch, M. H., Sayers, Z., Kuprin, S. & Zaccai, G. (1998). Protein hydration in solution: experimental observation by X-ray and neutron scattering. *Proc. Natl Acad. Sci. USA*, **95**, 2267–2272.
64. Kozin, M. B. & Svergun, D. I. (2001). Automated matching of high- and low-resolution structural models. *J. Appl. Crystallog.* **34**, 33–41.

Edited by R. Huber

(Received 28 March 2002; received in revised form 10 June 2002; accepted 14 June 2002)